

## Mass distributions for induced fission of different Hg isotopes

A. V. Andreev, G. G. Adamian, and N. V. Antonenko

*Joint Institute for Nuclear Research, 141980 Dubna, Russia*

(Received 20 June 2012; revised manuscript received 6 September 2012; published 11 October 2012)

With the improved scission-point model mass distributions are calculated for induced fission of different Hg isotopes with even mass numbers  $A = 180, 184, 188, 192, 196$ , and  $198$ . The calculated mass distribution and mean total kinetic energy of fission fragments are in good agreement with the existing experimental data. The asymmetric mass distribution of fission fragments of  $^{180}\text{Hg}$  observed in the recent experiment is explained. The change in the shape of the mass distribution from asymmetric to more symmetric is revealed with increasing  $A$  of the fissioning  $^A\text{Hg}$  nucleus, and reactions are proposed to verify this prediction experimentally.

DOI: [10.1103/PhysRevC.86.044315](https://doi.org/10.1103/PhysRevC.86.044315)

PACS number(s): 24.75.+i, 25.85.-w, 24.10.Pa

Since the discovery of nuclear fission this phenomenon has been intensively investigated. The mass distributions in the low-energy fission of actinides have been explored in detail. The asymmetric shape of the mass distribution is well known in the spontaneous, neutron-induced, and  $\beta$ -delayed fission of most actinide isotopes. Such an asymmetric shape was theoretically explained by taking into account the shell structure of the fragments [1–5]. During the past few decades new experimental techniques were developed to investigate the low-energy fission of lighter isotopes. Studies of the Coulomb-excited fission of radioactive nuclei revealed the predominance of symmetric fission in the light thorium to astatine region [6]. In the fission of stable targets with mass numbers  $A = 185$ – $210$  induced by protons and  $^3,4\text{He}$  the mass distribution was also found to be symmetric in most cases [7]. However, for several nuclei with  $A \approx 200$  the mass distribution looks symmetric but with a small dip on the top at small excitation energies [7]. Based on most of the experimental data, one could conclude that the asymmetric shape of the mass distribution in low-energy fission changes to a symmetric one with decreasing mass number of the fissioning nucleus. It was unexpected that in the recent experiment [8] on  $\beta$ -delayed fission of  $^{180}\text{Tl}$  the shape of the mass distribution was found to be clearly asymmetric. The explanation of this interesting result is a challenge for nuclear theory and a good test for the existing models of nuclear fission.

As shown with the stochastic approach of Ref. [9], the mass-asymmetry distribution reflects the detailed structure of the potential-energy surface in the scission region. The statistical scission-point model of Ref. [1] just relies on the assumption that statistical equilibrium is established at scission and the observable characteristics of the fission process are formed near the prescission configurations of the fissioning nucleus. With the modified scission-point model [10] we can describe the experimental data on fission of actinides: mass, charge, and kinetic energy distributions and neutron multiplicity distributions. With this model a new explanation of a bimodality effect in the fission of heavy actinides and the fine structure of the mass-energy distribution in the fission of  $^{236}\text{U}$  have been proposed. The model has been also extended to the description of ternary fission [11]. The advantage of our model is that it allows us to describe a large variety of experimental data with a fixed set of parameters and assumptions. The wide range of described fission observables and effects demonstrates the

predictive power of the model. In the present work we apply our model to the fission of lighter nuclei for describing the new experimental data [8] on asymmetric fission of  $^{180}\text{Hg}$ .

Here, we give a short description of the model; the details can be found in Refs. [10,11]. The fissioning nucleus at the scission point is modeled by two nearly touching coaxial spheroids—fragments of a dinuclear system with masses (charges)  $A_L$  ( $Z_L$ ) and  $A_H$  ( $Z_H$ ) of the light ( $L$ ) and heavy ( $H$ ) fragments, respectively.  $A = A_L + A_H$  ( $Z = Z_L + Z_H$ ) is the mass (charge) number of the fissioning nucleus. By taking into account volume conservation, the shape of the system is defined by the mass and charge numbers of the fragments, deformation parameters of the fragments,  $\beta_i$  ( $i = L, H$ ), and the interfragment distance  $R$ . The deformation parameter of each fragment is the ratio of the major and minor semi-axes of the spheroid,  $\beta_i = c_i/a_i$ . Here and further  $i$  denotes the light or heavy fragment of the dinuclear system. The case  $\beta_i = 1$  corresponds to a spherical shape for the fragment. For small values of  $\beta_i - 1$ , the following equality is valid:  $\beta_i \approx \beta_{2i} + 1$ , where  $\beta_{2i}$  is the parameter of quadrupole deformation of the  $i$ th fragment in the multiple expansion of the fragment shape.

The potential energy of the system,

$$\begin{aligned}
 U(A_i, Z_i, \beta_i, R, l) &= U^{\text{macro}}(A_i, Z_i, \beta_i, R, l) + \delta U^{\text{shell}}(A_i, Z_i, \beta_i), \\
 U^{\text{macro}}(A_i, Z_i, \beta_i, R, l) &= U_L^{LD}(A_L, Z_L, \beta_L) + U_H^{LD}(A_H, Z_H, \beta_H) \\
 &\quad + V^C(A_i, Z_i, \beta_i, R) + V^N(A_i, Z_i, \beta_i, R) \quad (1) \\
 &\quad + V^{\text{rot}}(A_i, Z_i, \beta_i, R, l) + U^{zpv}(A_i, Z_i), \\
 \delta U^{\text{shell}}(A_i, Z_i, \beta_i) &= \delta U_L^{\text{shell}}(A_L, Z_L, \beta_L) + \delta U_H^{\text{shell}}(A_H, Z_H, \beta_H),
 \end{aligned}$$

is the sum of the liquid-drop energies  $U_i^{LD}$  of each fragment, the energy of interaction of the fragments,  $V^C + V^N$ , the rotational energy  $V^{\text{rot}}$ , the energy  $U^{zpv}$  of zero-point vibrations, and the shell-correction terms  $\delta U_i^{\text{shell}}$ . The shell corrections are calculated with the Strutinsky method and the two-center shell model [12]; the damping of the shell corrections with excitation energy and angular momentum  $l$  is introduced in our model. The interaction energy consists of the Coulomb interaction  $V^C$  of two uniformly charged spheroids and nuclear interaction  $V^N$  in the form of a double folding of

nuclear densities and density-dependent Skyrme-type nucleon-nucleon forces [13]. For  $\beta$ -delayed and induced fission, we use zero and nonzero angular momenta  $l$ , respectively (see below). We related the energy  $U^{zpv} = E_i^{2+} \coth[E_i^{2+}/T(l)]$  of zero-point vibrations with the energies  $E_i^{2+}$  of the first  $2^+$  excited states of the fragments from Ref. [14]. The definition of the temperature  $T(l)$  is given below. Here, we use a simplification that for all deformations the zero-point vibration energies at zero temperature are equal to the  $E_i^{2+}$  energy at the ground-state deformation. However, our calculations show that the nucleus being stiffer in the ground state in comparison to the neighboring nuclei remains to be stiffer at large deformations. The shape dependence of zero-point vibrations of the nascent fragments is taken effectively into account through the shape-dependent temperature or excitation energy. At high excitation energy  $U^{zpv} = T(l)$  for all fragments.

All terms in Eq. (1) except for  $U^{zpv}$  depend on deformations of the fragments. For given deformations of the fragments the interaction potential has a potential minimum (pocket) as a function of the interfragment distance  $R$ . For calculation of the potential energy we take the value of the interfragment distance  $R = R_m$  corresponding to this minimum [ $U(A_i, Z_i, \beta_i, l) \equiv U(A_i, Z_i, \beta_i, R_m, l)$ ]. Depending on the masses of the fragments and their deformations the calculated distance between the tips of the spheroids is 0.5–1 fm.

Because thermodynamic equilibrium is postulated at the scission point, the excitation energy of the nuclear system at scission is calculated as a difference between the potential energy  $U_{CN}(A, Z, \beta, l)$  of the compound nucleus (fissioning nucleus) and the potential energy  $U(A_i, Z_i, \beta_i, l)$  of the dinuclear system at the scission point plus the initial excitation energy  $E_{CN}^*(l)$  of the compound nucleus:  $E^*(l) = U_{CN}(A, Z, \beta, l) - U(A_i, Z_i, \beta_i, l) + E_{CN}^*(l)$ . The temperature is calculated as  $T(l) = \sqrt{E^*(l)/a}$ , where  $a = A/12$  is the level density parameter in the Fermi-gas model. The yield of a particular scission configuration with given mass and charge numbers and deformation parameters of the fragments is proportional to the exponential Boltzmann factor:

$$Y(A_i, Z_i, \beta_i, l) \sim \exp\left\{-\frac{U(A_i, Z_i, \beta_i, l)}{T(l)}\right\}. \quad (2)$$

$$\langle \text{TKE} \rangle(A_i, Z_i) = \frac{\sum_{l=0}^{l_{\max}} (2l+1) \int \text{TKE}(A_i, Z_i, \beta_i, l) \exp\left\{-\frac{U(A_i, Z_i, \beta_i, l)}{T(l)}\right\} d\beta_L d\beta_H}{\sum_{l=0}^{l_{\max}} (2l+1) \int \exp\left\{-\frac{U(A_i, Z_i, \beta_i, l)}{T(l)}\right\} d\beta_L d\beta_H}, \quad (4)$$

where

$$\text{TKE}(A_i, Z_i, \beta_i, l) = V^C(A_i, Z_i, \beta_i, R_b) + V^N(A_i, Z_i, \beta_i, R_b) + V_{\text{rel}}^{\text{rot}}(A_i, Z_i, \beta_i, l), \quad (5)$$

$$V_{\text{rel}}^{\text{rot}}(A_i, Z_i, \beta_i, l) = \frac{\hbar^2 f l (f l + 1)}{2\mu R_b^2}, \quad (6)$$

$$f = \frac{\mu R_m^2}{\mathfrak{S}_L + \mathfrak{S}_H + \mu R_m^2}. \quad (7)$$

For given mass and charge split, the potential energy of the dinuclear system at the scission point is a function of deformations of the fragments [the potential energy surface (PES)]. Due to the Coulomb interaction between the fragments, the deformation parameters corresponding to the minimum in PES are larger than in the ground states of nuclei fragments, which indicates that the fragments at the scission point are significantly deformed. To obtain the relative mass distribution as a function of the mass number of one of the fragments in the fission of a compound nucleus with mass and charge numbers  $A$  and  $Z$ , one should integrate expression (2) over  $Z_L$ ,  $\beta_L$ , and  $\beta_H$ , sum over  $l$ , and take into account that  $A_H = A - A_L$  and  $Z_H = Z - Z_L$ :

$$Y(A_L) = \frac{\sum_{l=0}^{l_{\max}} (2l+1) \int \exp\left\{-\frac{U(A_i, Z_i, \beta_i, l)}{T(l)}\right\} dZ_L d\beta_L d\beta_H}{\sum_{l=0}^{l_{\max}} (2l+1) \int \exp\left\{-\frac{U(A_i, Z_i, \beta_i, l)}{T(l)}\right\} dA_L dZ_L d\beta_L d\beta_H}. \quad (3)$$

The distribution (3) is normalized to unity. The value of the angular momentum  $l$  is limited by either the kinetic angular momentum  $\hbar l_{\text{kin}} = R_b \sqrt{2\mu(E_{\text{c.m.}} - V_b)}$  [where  $R = R_b$  is the position of the Coulomb barrier with height  $V_b = V^C(A_i, Z_i, \beta_i = 0, R = R_b) + V^N(A_i, Z_i, \beta_i = 0, R = R_b)$  in the entrance channel,  $\mu = m_0 A_L A_H / (A_L + A_H)$  is the reduced mass parameter, and  $m_0$  is the nucleon mass] or by the calculated critical angular momentum  $l_{\text{cr}}$  in the entrance channel, depending on which one is smaller:  $l_{\max} = \min\{l_{\text{kin}}, l_{\text{cr}}\}$ .

The scission-point model is also suitable for describing the total kinetic energy (TKE) of the fission fragments. We calculate the TKE by supposing that all interaction energy at the scission point transforms after fission into the kinetic energy of the fission fragments. Therefore, the value of the TKE strongly depends on the deformations of the fragments at the scission point. The smaller the deformations of the fragments and the larger the Coulomb repulsion, the larger the TKE will be. The mean value of the total kinetic energy for a particular binary splitting is calculated by averaging over deformations of the fragments on the PES:

Here,  $\mathfrak{S}_L$  and  $\mathfrak{S}_H$  denote the moments of inertia of the fragments.

The average value of the TKE of the fission fragments can be found from  $\langle \text{TKE} \rangle(A_i, Z_i)$  by averaging over all binary systems:

$$\overline{\text{TKE}} = \int \langle \text{TKE} \rangle(A_i, Z_i) Y(A_i, Z_i) dA_L dZ_L, \quad (8)$$

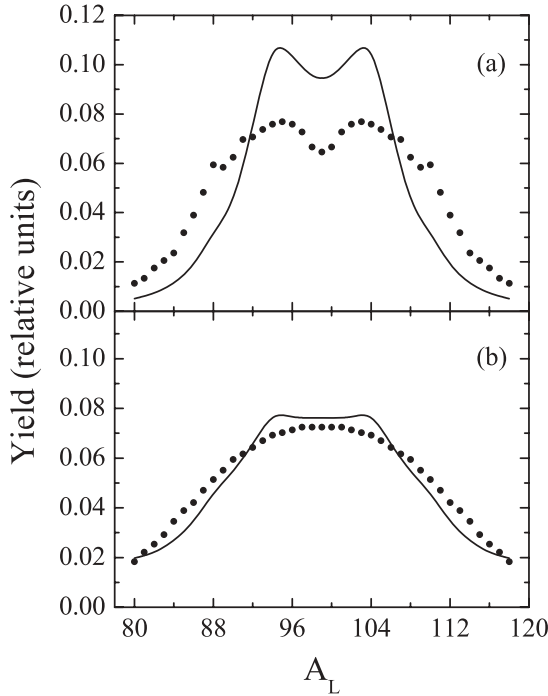


FIG. 1. Calculated (solid line) mass distribution of fission fragments in comparison with the experimental data [7] (points) for induced fission of  $^{198}\text{Hg}$  in the reaction  $^{197}\text{Au}(p, f)$  at  $E_p = 22.4$  MeV (a) and in the reaction  $^{194}\text{Pt}(\alpha, f)$  at  $E_\alpha = 50.4$  MeV (b).

where

$$Y(A_i, Z_i) = \frac{\sum_{l=0}^{l_{\max}} (2l+1) \int \exp\left\{-\frac{U(A_i, Z_i, \beta_i, l)}{T}\right\} d\beta_L d\beta_H}{\sum_{l=0}^{l_{\max}} (2l+1) \int \exp\left\{-\frac{U(A_i, Z_i, \beta_i, l)}{T}\right\} dA_L dZ_L d\beta_L d\beta_H} \quad (9)$$

We performed calculations of mass distributions for isotopes of Hg with mass numbers  $A = 180, 184, 188, 192, 196$ , and  $198$ . As a first step, the calculations were restricted only to even-even fission fragments, which mainly define the shape of the mass distribution. The inclusion of the odd-even and odd-odd fission fragments can only smooth out a little the distribution but cannot appreciably change its shape. In order to obtain a smooth curve and to simulate the experimental uncertainty of the extraction of the fission-fragment mass number, each calculated yield was smeared by a Gaussian with width  $\sigma_{A_L} = 1.5$  amu.

To test our fission model in the mass region under consideration, we calculated the mass distribution for the reactions  $^{197}\text{Au}(p, f)$  at the energy of a proton of 22.4 MeV and  $^{194}\text{Pt}(\alpha, f)$  at the energy of an  $\alpha$  particle of 50.4 MeV [where the fissioning compound nucleus is  $^{198}\text{Hg}$  with  $E_{CN}^*(l=0) = 29.4$  MeV and  $E_{CN}^*(l=0) = 49.0$  MeV, respectively]. Figure 1 shows a comparison of our calculations with the experimental data [7]. The calculated and experimental distributions have a similar shape with a dip at the top for the reaction  $^{197}\text{Au}(p, f)$ , the maxima almost coincide, but the calculated distribution is slightly narrower than the experimental one.

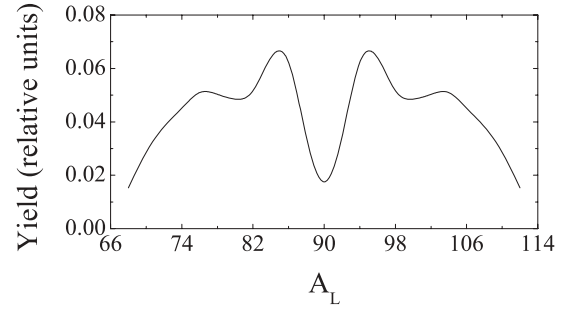


FIG. 2. Calculated mass distribution of fission fragments for  $\beta$ -delayed fission of  $^{180}\text{Tl}$  (with the fissioning nucleus being  $^{180}\text{Hg}$ ).

For the reaction  $^{194}\text{Pt}(\alpha, f)$  this dip almost disappears due to the larger excitation energy, which is in agreement with the experimental data. These examples demonstrate the validity of our treatment of the excitation-energy-dependent shell effects.

For  $\beta$ -delayed fission of  $^{180}\text{Tl}$  [8], the excitation energy  $E_{CN}^*(l=0)$  of the fissioning nucleus  $^{180}\text{Hg}$  does not exceed 10.44 MeV. The mass distribution of fission fragments is presented in Fig. 2. We obtained a clearly asymmetric mass distribution with average masses of the light and heavy fragments of about 80 and 100, respectively, which is in agreement with the experimental data [8]. The calculated  $\overline{\text{TKE}} = 136$  MeV is also in good agreement with the experiment [8].

It is convenient to analyze the obtained results for fission of  $^{180}\text{Hg}$  by comparison of the PES of different mass/charge splits (Fig. 3). If one excludes the shell-correction terms from Eq. (1) the PES will have a minimum at deformations of the fragments of about  $\beta_i = 1.6$ . These  $\beta_i$  are larger than the ground-state deformations of the corresponding nuclei because of polarization. In the fission of  $^{180}\text{Hg}$  the symmetric scission configuration is  $^{90}\text{Zr} + ^{90}\text{Zr}$ . The shell correction for  $^{90}\text{Zr}$  has a negative value,  $\delta U_i^{\text{shell}} \approx -2$  MeV, near  $\beta_i = 0$ ; at larger deformations it becomes positive; at  $\beta_i = 1.6$  it is equal to  $\delta U_i^{\text{shell}} \approx 1$  MeV, then it grows further, and at  $\beta_i = 1.85$  it reaches  $\delta U_i^{\text{shell}} \approx 4$  MeV. In contrast, the shell corrections for nonmagic nuclei in the scission configurations Kr + Ru and Se + Pd are usually positive at small deformations ( $\delta U_L^{\text{shell}} \approx 2.5$  MeV and  $\delta U_H^{\text{shell}} \approx 1.5$  MeV) and have zero or slightly negative values in the region around  $\beta_i = 1.6$ . Because of these shell effects, the minimum is narrow for  $^{90}\text{Zr} + ^{90}\text{Zr}$ , while for  $^{76}\text{Se} + ^{104}\text{Pd}$ , where the shell effects are weaker, it is wide (see Fig. 3).

Figure 4 demonstrates the change of potential energy of the binary systems  $^{90}\text{Zr} + ^{90}\text{Zr}$  and  $^{76}\text{Se} + ^{104}\text{Pd}$  along the trajectory on the PES over the local minima starting from the point  $\beta_L = \beta_H = 1$ . Here,  $\beta$  denotes the deviation from the point  $\beta_L = \beta_H = 1$  along this trajectory on the plane  $(\beta_L, \beta_H)$ . Due to the influence of the term  $U^{zpv}$  (high value of  $E_{L,H}^{2+}$  for  $^{90}\text{Zr}$ ), the  $U^{\text{macro}}$  energy at the minimum has a smaller value for the asymmetric split  $^{76}\text{Se} + ^{104}\text{Pd}$  than for the symmetric split  $^{90}\text{Zr} + ^{90}\text{Zr}$ . Since at the deformations of the minima the shell corrections are comparable for the splits  $^{90}\text{Zr} + ^{90}\text{Zr}$  and  $^{76}\text{Se} + ^{104}\text{Pd}$ , this leads to a larger yield of the split Se + Pd. In addition, the difference in the widths of the minima for  $^{90}\text{Zr} + ^{90}\text{Zr}$  and  $^{76}\text{Se} + ^{104}\text{Pd}$  strengthens the difference in the yields of these splits. Due to the integration in Eq. (3), the

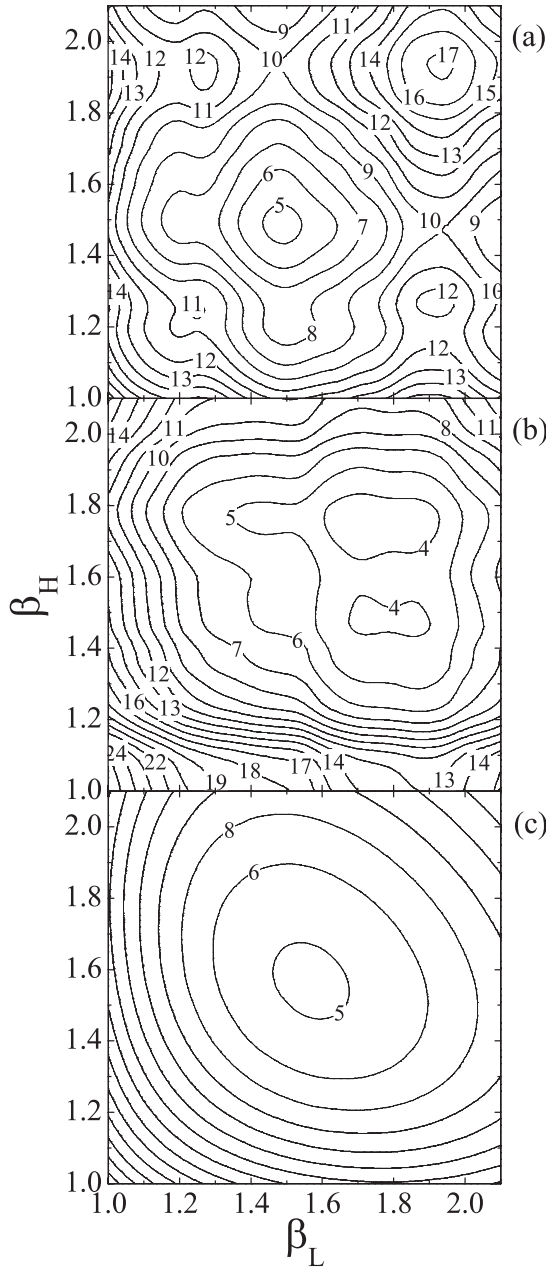


FIG. 3. Calculated potential energy at the scission point as a function of deformations of the fragments in the binary systems  $^{90}\text{Zr} + ^{90}\text{Zr}$  (a) and  $^{76}\text{Se} + ^{104}\text{Pd}$  (b). The energy is given in MeV relative to the energy of the fissioning nucleus  $^{180}\text{Hg}$ . (c) The potential energy calculated without the shell-correction terms in Eq. (1) for the binary system  $^{90}\text{Zr} + ^{90}\text{Zr}$ .

wide minimum for  $^{76}\text{Se} + ^{104}\text{Pd}$  results in a larger yield of corresponding fragments.

Figure 5 shows a change in the shape of the mass distribution from asymmetric to more symmetric with increasing mass number  $A$  of the fissioning nucleus  $^A\text{Hg}$ . While the mass distribution is quite asymmetric for  $^{180}\text{Hg}$  and  $^{184}\text{Hg}$ , for  $^{188}\text{Hg}$  the asymmetry is less pronounced, and for  $^{192}\text{Hg}$  and  $^{196}\text{Hg}$  the mass distribution looks more symmetric but with a dip on the top similar to that observed experimentally in the

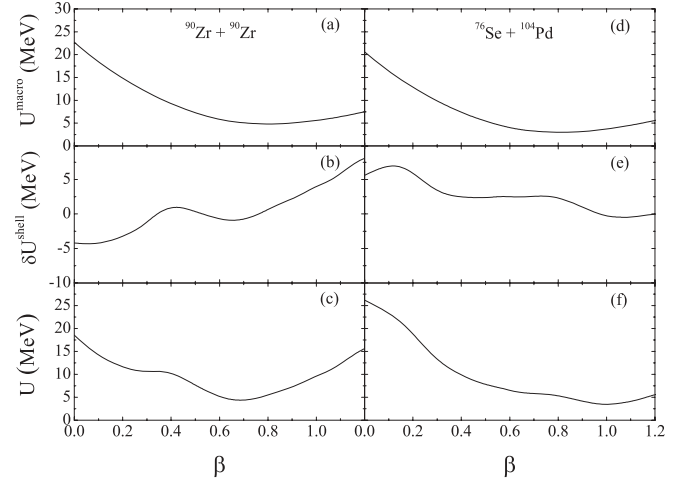


FIG. 4. The calculated energies (in MeV)  $U^{\text{macro}}$  [(a) and (d)],  $\delta U^{\text{shell}}$  [(b) and (e)], and  $U$  [(c) and (f)] along the local minima on the PES as functions of deviation from the point  $\beta_L = \beta_H = 1$  on the plane  $(\beta_L, \beta_H)$  for the binary systems  $^{90}\text{Zr} + ^{90}\text{Zr}$  [(a), (b), and (c)] and  $^{76}\text{Se} + ^{104}\text{Pd}$  [(d), (e), and (f)] formed at the scission point during the  $\beta$ -delayed fission of  $^{180}\text{Tl}$ .

fission of  $^{198}\text{Hg}$  [7] (Fig. 5). This result slightly differs from the results of Ref. [15], where the mass distribution was found to be asymmetric for  $^{180-188}\text{Hg}$  with the asymmetry increasing with increasing mass number of the fissioning Hg isotope. In our model, with increasing mass of the fissioning nucleus, the fragments of symmetric scission configurations deviate from the magic  $^{90}\text{Zr}$ , and the role of strong shell effects at symmetric splits decreases. Thereby, in the heavy isotopes of Hg the shape of the mass distribution is generally defined by the liquid-drop part of the energy, and we obtain more symmetric mass distributions. For instance, let us compare the symmetric and asymmetric fragmentations in the fission of  $^{180}\text{Hg}$  (Fig. 4) and  $^{198}\text{Hg}$  (Fig. 6). In the case of  $^{198}\text{Hg}$  the energies  $U^{\text{macro}}$  and  $\delta U^{\text{shell}}$  ( $U^{\text{macro}} \gg |\delta U^{\text{shell}}|$ ) in the deformation minimum for the symmetric split  $\text{Zr} + \text{Zr}$  are smaller than the ones for the asymmetric split  $\text{Se} + \text{Pd}$ . In the case of  $^{180}\text{Hg}$  one can see the opposite behavior.

Figure 5 demonstrates the influence of the excitation energy of the fissioning nucleus  $^A\text{Hg}$  on the shape of the mass distribution. The excitation energy reduces the shell effects and smooths out the shape of the mass distribution. However, for some isotopes the influence of the excitation energy is rather weak. For example, in the case of  $^{180}\text{Hg}$  the mass distribution has a pronounced asymmetric shape even at the excitation energy  $E_{CN}^* = 64.2$  MeV [8].

Figure 7 demonstrates the calculated dependence of

$$\langle \text{TKE} \rangle (Z_i) = \int \langle \text{TKE} \rangle (A_i, Z_i) Y(A_i, Z_i) dA_L \quad (10)$$

on the atomic mass number of the light fission fragment for the induced fission of nuclei  $^{180,196}\text{Hg}$  at a bombarding energy 10 MeV above the Coulomb barrier ( $E_{c.m.} = V_b + 10$  MeV). The curve rises fast for  $^{180}\text{Hg}$  due to its approaching the compact symmetric scission configuration  $^{90}\text{Zr} + ^{90}\text{Zr}$ , while for  $^{196}\text{Hg}$

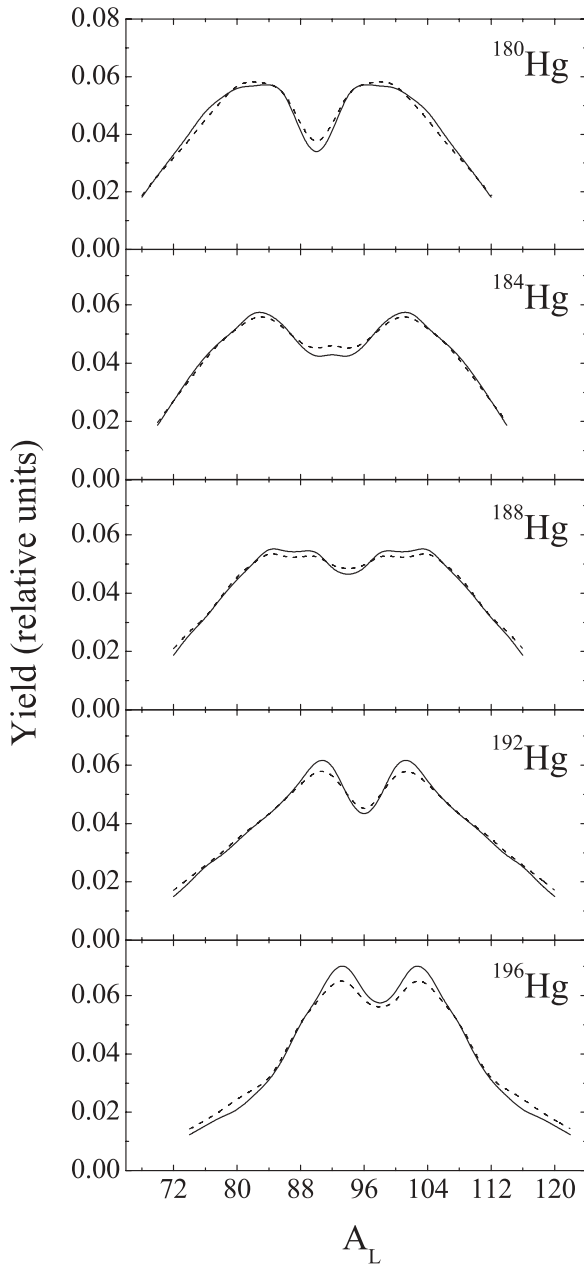


FIG. 5. Calculated mass distributions of fission fragments for induced fission of  $^{180,184,188,192,196}\text{Hg}$  with impact energies of 10 MeV [solid lines,  $E_{CN}^*(l=0) = 44.2, 43.9, 49.7, 62.4,$  and  $56.0$  MeV for  $^{180,184,188,192,196}\text{Hg}$ , respectively] and 30 MeV [dashed lines,  $E_{CN}^*(l=0) = 64.2, 63.9, 69.7, 82.4,$  and  $76.0$  MeV for  $^{180,184,188,192,196}\text{Hg}$ , respectively] above the corresponding Coulomb barriers for spherical nuclei (see text).

the curve is almost horizontal because the symmetric configuration  $^{98}\text{Zr} + ^{98}\text{Zr}$  contains the nonmagic nuclei. The value of  $\langle\text{TKE}\rangle$  is generally defined by the position of the minimum of the PES. Because of shell effects, the minimum of the potential energy of the scission configuration  $^{90}\text{Zr} + ^{90}\text{Zr}$  is shifted from the liquid-drop minimum  $\beta_i = 1.6$  to smaller deformations  $\beta_i = 1.5$ , which leads to the gain in  $\langle\text{TKE}\rangle$ . In the scission configurations consisting of nonmagic nuclei the minimum of

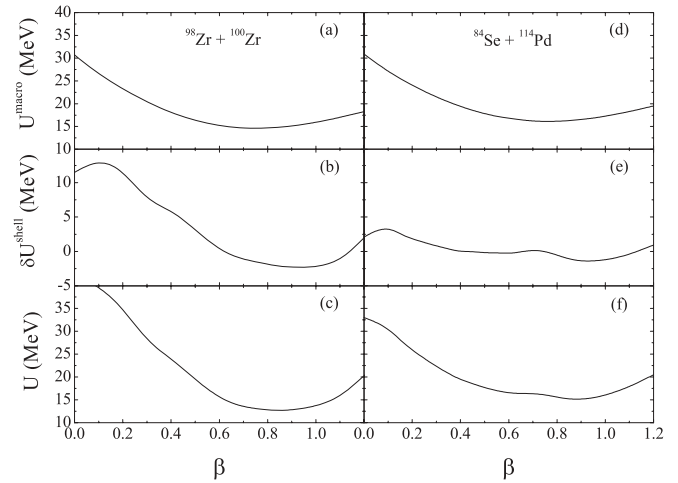


FIG. 6. The same as in Fig. 4, but for the binary systems  $^{98}\text{Zr} + ^{100}\text{Zr}$  [(a), (b), and (c)] and  $^{84}\text{Se} + ^{114}\text{Pd}$  [(d), (e), and (f)] formed at the scission point during proton-induced fission of  $^{197}\text{Au}$  at  $E_p = 22.4$  MeV.

the potential energy corresponds to a liquid-drop minimum with deformations around  $\beta_i = 1.6$ – $1.65$ .

To study the fission properties of all considered isotopes  $^{180}\text{Hg}$ ,  $^{184}\text{Hg}$ ,  $^{188}\text{Hg}$ ,  $^{192}\text{Hg}$ , and  $^{196}\text{Hg}$  (Fig. 5), we propose induced fission reactions at bombarding energies 10 and 30 MeV above the corresponding Coulomb barriers  $V_b$  for spherical nuclei:  $^{36}\text{Ar} + ^{144}\text{Sm} \rightarrow ^{180}\text{Hg}$  ( $V_b = 126.2$  MeV,  $l_{\text{max}} = 44$  and  $61$ ),  $^{40}\text{Ar} + ^{144}\text{Sm} \rightarrow ^{184}\text{Hg}$  ( $V_b = 124.55$  MeV,  $l_{\text{max}} = 46$  and  $71$ ),  $^{40}\text{Ar} + ^{148}\text{Sm} \rightarrow ^{188}\text{Hg}$  ( $V_b = 123.9$  MeV,  $l_{\text{max}} = 46$  and  $66$ ),  $^{32}\text{S} + ^{160}\text{Gd} \rightarrow ^{192}\text{Hg}$  ( $V_b = 114.4$  MeV,  $l_{\text{max}} = 42$  and  $63$ ), and  $^{36}\text{S} + ^{160}\text{Gd} \rightarrow ^{196}\text{Hg}$  ( $V_b = 112.8$  MeV,  $l_{\text{max}} = 45$  and  $70$ ).

Our model gives a good description of the reactions  $^{197}\text{Au}(p, f)$ ,  $^{194}\text{Pt}(\alpha, f)$ , and of the recent experiment [8] where the asymmetric mass distribution in the fission of  $^{180}\text{Hg}$  was observed. The latter unexpected effect required a theoretical explanation and the present work provides it. The results of our calculations confirm the importance of the shell structure and, correspondingly, deformation effects in the fission process.

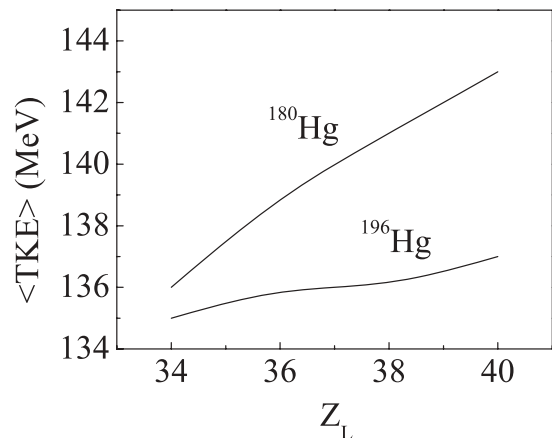


FIG. 7.  $\langle\text{TKE}\rangle(Z_i)$  for the induced fission of  $^{180}\text{Hg}$  and  $^{196}\text{Hg}$  as functions of the atomic mass number of the light fragment.

The account of different fragment deformations at the scission point is necessary for the correct description of the mass distributions and kinetic energy of the fission fragments. We made a prediction of the change in the shape of the mass distribution from asymmetric to more symmetric with increasing mass number of the fissioning Hg isotope from

$A = 180$  to  $A = 196$ , and we proposed the reactions to verify this prediction experimentally.

We thank Dr. A. N. Andreyev for fruitful discussions. This work was supported by DFG (Bonn) and RFBR (Moscow).

- 
- [1] B. D. Wilkins, E. P. Steinberg, and R. R. Chasman, *Phys. Rev. C* **14**, 1832 (1976).
- [2] P. Möller, D. G. Madland, A. J. Sierk, and A. Iwamoto, *Nature (London)* **409**, 785 (2001).
- [3] F. Gönnenwein, in *The Nuclear Fission Process*, edited by C. Wagemans (CRC Press, Boca Raton, FL, 1991).
- [4] H. L. Hall and D. C. Hoffman, *J. Radiol. Nucl. Chem.* **142**, 53 (1990).
- [5] Yu. Ts. Oganessian, *J. Phys. G* **34**, R165 (2007).
- [6] K.-H. Schmidt *et al.*, *Nucl. Phys. A* **693**, 169 (2001); **665**, 221 (2000).
- [7] M. G. Itkis *et al.*, *Sov. J. Nucl. Phys.* **52**, 601 (1990); **53**, 757 (1991).
- [8] A. N. Andreyev *et al.*, *Phys. Rev. Lett.* **105**, 252502 (2010); J. Elseviers *et al.*, to be published in *Phys. Rev. C*.
- [9] J. Randrup, P. Möller, and A. J. Sierk, *Phys. Rev. C* **84**, 034613 (2011).
- [10] A. V. Andreev *et al.*, *Eur. Phys. J. A* **22**, 51 (2004); **26**, 327 (2005).
- [11] A. V. Andreev *et al.*, *Eur. Phys. J. A* **30**, 579 (2006).
- [12] J. Maruhn and W. Greiner, *Z. Phys.* **251**, 431 (1972).
- [13] G. G. Adamian *et al.*, *Int. J. Mod. Phys. E* **5**, 191 (1996).
- [14] S. Raman *et al.*, *At. Data Nucl. Data Tables* **78**, 1 (2001).
- [15] P. Möller, J. Randrup, and A. J. Sierk, *Phys. Rev. C* **85**, 024306 (2012).